

Technical Section

Accurate and robust registration of low overlapping point clouds[☆]Jieyin Yang ^{a,b}, Mingyang Zhao ^{c,d}, Yingrui Wu ^{d,b}, Xiaohong Jia ^{a,b,*}^a KLM, Academy of Mathematics and Systems Science, Chinese Academy of Sciences, China^b University of Chinese Academy of Sciences, Beijing, China^c CAIR Hong Kong Institute of Science & Innovation, Chinese Academy of Sciences, China^d State Key Laboratory of Multimodal Artificial Intelligence Systems (MAIS), Institute of Automation, Chinese Academy of Sciences, China

ARTICLE INFO

Keywords:

Point cloud registration

ICP

HMRF

Low overlapping

Outliers

ABSTRACT

Point cloud registration has various applications within the *computer-aided design* (CAD) community, such as model reconstruction, retrieving, and analysis. Previous approaches mainly deal with the registration with a high overlapping hypothesis, while few existing methods explore the registration between low overlapping point clouds. However, the latter registration task is both challenging and essential, since the weak correspondence in point clouds usually leads to an inappropriate initialization, making the algorithm get stuck in a local minimum. To improve the performance against low overlapping scenarios, in this work, we develop a novel algorithm for accurate and robust registration of low overlapping point clouds using optimal transformation. The core of our method is the effective integration of *geometric features* with the probabilistic model *hidden Markov random field*. First, we determine and remove the outliers of the point clouds by modeling a hidden Markov random field based on a high dimensional feature distribution. Then, we derive a *necessary and sufficient condition* when the symmetric function is minimized and present a new curvature-aware symmetric function to make the point correspondence more discriminative. Finally, we integrate our curvature-aware symmetric function into a geometrically stable sampling framework, which effectively constrains unstable transformations. We verify the accuracy and robustness of our method on a wide variety of datasets, particularly on low overlapping range scanned point clouds. Results demonstrate that our proposed method attains better performance with higher accuracy and robustness compared to representative state-of-the-art approaches.

1. Introduction

Point cloud registration is a fundamentally important problem in CAD and computer graphics [1,2]. It can be utilized for various applications, such as 3D reconstruction [3–6], CAD model retrieving [7], as well as scene modeling and cultural heritage management [8,9]. Given two partial range scans, the goal is to seek a *spatial transformation* comprising a 3D rotation matrix $\mathbf{R} \in \text{SO}(3)$ ¹ and a translation vector $\mathbf{t} \in \mathbb{R}^3$ to optimally align them into a common reference system [10].

Iterative closest point (ICP) [11,12] is a milestone and has become the most frequently used method for point cloud registration. It iteratively builds up the point proximity and calculates the transformation parameters via *singular value decomposition* (SVD) [13] or *dual quaternion* [14]. Benefiting from its simplicity and high efficiency, ICP becomes the de-facto standard within the industrial community. However, there still exist several challenges in the development of a versatile or robust ICP.

The primary challenge is the accurate registration of low overlapping point clouds caused by large perspective variations. As ICP highly depends on the initialization or correspondence, low overlapping inputs usually make it converge to a local minimum, as shown in Fig. 1. Although there are many variants of ICP in the literature, for instance, the point-to-plane metric is designed to enhance the point-to-point computation [15,16], the L_p minimization or *M-estimators* are used to improve its robustness against outliers [17–20], while the consideration of local accuracy and global consistency extends the registration algorithms of two objects to multi-view registration [21,22]. To the best of our knowledge, few approaches [23,24] have been explored to tackle this challenging low overlapping problem.

Recently, the *hidden Markov random field model* (HMRF) [25] is customized for point cloud registration [23], which shows potential power for dealing with low overlapping scans. However, it merely minimizes the point-to-point distance and ignores the 3D geometric features of point clouds, which empirically enables higher accuracy and more stable performance.

[☆] This article was recommended for publication by Mirela Ben-Chen.

* Corresponding author.

E-mail address: xhjia@amss.ac.cn (X. Jia).

¹ $\text{SO}(3) := \{\mathbf{R} \in \mathbb{R}^{3 \times 3} | \mathbf{R}\mathbf{R}^T = \mathbf{R}^T\mathbf{R} = \mathbf{I}_3, \det \mathbf{R} = 1\}$.

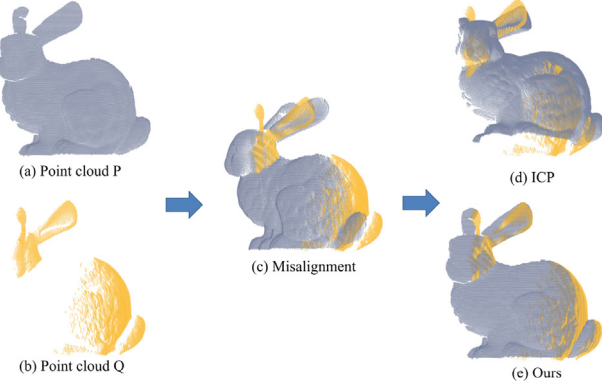


Fig. 1. Illustration of low overlapping point cloud registration. ICP tends to get stuck into the local minimum due to the insufficient correspondence, whereas our proposed method returns highly accurate registration.

To explore geometric features and involve them into the HMRF framework, in this work, we propose a new method for low overlapping point cloud registration, which attains appealing results in both accuracy and robustness. An overview of our method is shown in Fig. 2. Instead of using the spatial distance as the single criterion when modeling the HMRF, we also take geometric features such as the planarity, anisotropy, and curvature into consideration. This indeed gives a high dimensional feature distribution. Compared with distance residual, these features are more discriminative and effective, which help estimate the overlapping region more precisely, as is shown in Fig. 2(b). In terms of the metric function, we utilize the symmetric distance including both normals and curvatures of data points for error measurement. We demonstrate that the proposed curvature-aware symmetric function results in more meaningful and distinguished punishment. Additionally, we point out that the previous point-to-plane metric is a special case of our newly defined objective function around the plane point, *i.e.*, the point whose neighboring local surface is a plane. Based on this curvature-aware metric, we further use linear approximation of the objective function and incorporate it into a geometrically stable sampling framework, as presented in Fig. 2(c), in which we leverage the matrix condition number to attain stable transformations. Fig. 2(d) shows the intermediate result of our method after conducting five iterations and the final registration result is presented in Fig. 2(e).

We conduct extensive experiments to validate the performance of the proposed method and compare it with representative state-of-the-art approaches on a wide variety of benchmark datasets. Results demonstrate that our method attains several salient advantages than competitors, *i.e.*, more accurate for low overlapping point cloud registration, as well as more robust against noise and outliers. To summarize, the main technical contributions of this work are as follows:

- We propose a novel method toward low overlapping point cloud registration via the integration of geometric features and HMRF, which attains superior performance in both accuracy and robustness.
- We deduce an optimal condition of the symmetric function and incorporate curvature geometry into it to make the optimization more discriminative.
- We derive a curvature-aware point pair sampling process, which effectively improves the transformation stability.

The reminder of this paper is organized as follows: Section 2 reviews the rigid point cloud registration methods from four categories. The contributions of our methodology are presented in Section 3. We perform extensive experiments to assess the performance of our designed algorithm in Section 4. Section 5 concludes our study, discusses its limitations, and points out possible extensions.

2. Related work

Due to the importance of point cloud registration on practical applications, extensive pioneer work have been made over the past several

decades. The readers are referred to [26,27] for more comprehensive studies. Here, we put our focus on rigid point cloud registration.

2.1. ICP-based methods

ICP proposed by [11] is one of the most famous point cloud registration algorithm. After its introduction, a lot of efforts have been devoted to improve its efficiency and robustness. The most popular modification for efficiency improvement is to refine the objective function of the original point-to-point distance by the point-to-plane manner by [12], in which the l_2 distance from source points to the tangent planes of their corresponding points were calculated. [28] estimated the local surface around each point as a quadratic surface and introduced a squared distance function, which was then demonstrated theoretically and experimentally by [29] to have higher stability than the point-to-plane ICP. Recently, [30] raised a symmetric objective function taking normals of the point pairs into consideration, achieving the same simplicity and computational efficiency as the point-to-plane metric, yet with a wider convergence basin.

Besides the improvement of convergence speed, many work focused on the robustness promotion against noise and outliers. Among these algorithms, a popular attempt is to use robust estimators. [31] revised the original l_2 norm of ICP as l_1 norm to increase the algorithm's sparsity and robustness. Moreover, sparse ICP raised up by [32] had their objective function based on the l_p norm with $p \in (0, 1)$ and optimized it by the iterative framework *Alternating Direction Method of Multipliers* (ADMM). Another line of work invokes *M-estimators* to depress the influence of large residuals. For example, fast global registration by [33] took the Geman-McClure estimator as the penalty function and conducted the alignment in one single stage without the closest point queries, whereas [19] utilized the Welsch function to enhance the robustness. Although these work are capable of relieving the outlier influence, when facing partially overlapping scenarios, they directly regard the points in non overlapping regions as outliers, hence are prone to misalignment. Several work had made attempts on low overlapping situations. For instance, [34] discarded point pairs whose distances surpass a certain threshold. Based on the neighbor priors, [23] distinguished the inliers in overlapping regions from outliers by modeling a hidden Markov random field, which showed advantages on moderate overlapping.

2.2. Statistics-based methods

Apart from the variants of ICP, statistical models are also customized for point cloud registration such as the *Gaussian Mixture Models* (GMM). [35] treated the source and the target point clouds as two GMMs, then the alignment problem was transformed into minimizing the discrepancy of the two probabilistic distributions under the KL divergence, while [36] directly minimized the l_2 distance. Instead, coherent point drift (CPD) [37] described one of the point clouds as GMM, while the second set was realized via the *maximum likelihood estimation*. To encode more information into the statistical framework, [38] combined color feature with CPD together and designed a color-guided probabilistic registration method. Nevertheless, this algorithm is limited to the colorful point cloud registration task. To improve the robustness of statistical methods against the point density variation, [39] modeled the underlying structure of the scene as a potential probability distribution and put forward a density adaptive point set registration method. In order to guarantee the convergence of CPD algorithm and overcome the shortcoming that CPD was relatively sensitive to rotation, [40] formulated coherent point drift in a Bayesian setting and leveraged variational inference for the transformation solving. To solve the registration problem of cross-modality data, [41] formulated the cross-modality registration problem as a consistent clustering process and performed registration through hierarchical steps. Since statistical methods are based on the soft correspondence with probability, they are intrinsically robust. However, compared with ICP, these approaches usually have higher computational complexity.

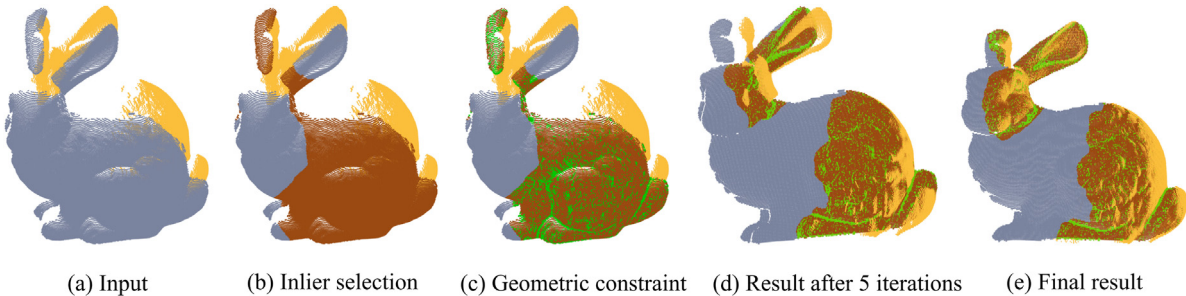


Fig. 2. Overview of the proposed framework: (a) Input point clouds. The yellow one and blue one represent the source P and the target Q , respectively. (b) Overlapping region estimation. Red point cloud represents the inliers in the overlapping region. (c) Geometric constraint of the inliers. Green point cloud represents the points selected by the curvature constraint and the point-pair sampling strategy. (d) Intermediate result after 5 iterations. (e) Final result when the iterations converge.

2.3. Correspondence-based methods

The correspondence-based method, represented by random sample consensus (RANSAC) algorithm, is also a very commonly used point cloud registration framework. RANSAC [42] is a general parameter estimation method designed to handle a significant proportion of outliers in the input data by alternatively performs minimal subset sampling and model fitting. With the introduction of RANSAC, many RANSAC-variant algorithms have been proposed to improve its sampling and model fitting. For example, n-adjacent points sample consensus (NAPSAC) [43] proposed a sampling strategy based on the assumption that inliers will tend to be closer to one another than outliers. This strategy enhances the algorithm's robustness in the presence of a high outliers. Progressive NAPSAC (P-NAPSAC) [44] combined the benefits of local and global sampling by selecting samples from gradually growing neighborhoods, which improved the efficiency of the RANSAC-based algorithm. [45] partitioned the complete seven-parameter registration problem into three subproblems and introduced a one-point RANSAC algorithm to estimate the scale and translation parameters. Graph enhanced sample consensus (GESAC) [46] generated a much larger subset allowing outliers in sampling step and used max-pooling graph matching strategy to remove potential outliers in the subset to improve the robustness of the algorithm under high outliers. Quadratic-time GORE (QGORE) [47] employed a voting idea based on geometric consistency for upper bound estimation to maintain the globally optimal solution, significantly enhancing efficiency of registration. While the correspondence-based method is capable of handling point clouds with outliers, it lacks robustness when registering point clouds with low overlapping regions. This is primarily due to the challenge of accurately predicting the overlapping regions of point clouds in advance, which makes it difficult to set appropriate thresholds for distinguishing inliers from outliers.

2.4. Deep-learning-based methods

With the advances of deep learning in recent years, people have tried applying neural networks for 3D point cloud registration. The typical idea is to replace main steps of the traditional pipeline in point cloud registration with learning-based modules. To be specific, [48] combined PointNet [49] with Lucas-Kanade (LK) algorithm [50] into a trainable deep neural network named PointNetLK. [51] implemented ICP algorithm from a deep learning perspective, provided a simple structure to predict the relative position of two point clouds, and relieved the local optimal problem in the classical ICP pipeline. [52] presented an end-to-end point cloud registration framework, in which the learned matching probability was used to generate corresponding points rather than selecting them from existing point pairs. [53] developed a differentiable framework for registration which contained three

modules. BUFFER [54] utilized both point-wise and patch-wise registration techniques to create a network consisting of a Point-wise Learner, Patch-wise Embedder, and Inlier Generator; this network efficiently balanced the accuracy, efficiency, and generalizability in point cloud registration. RORNet [24] proposed a partial-to-partial registration network, extracting reliable representations of the estimated overlapping area before registration to reduce the side effects of overlap estimation errors. Learning-based methods are able to represent features more effectively, nevertheless, they usually require longstanding training. As far as we know, the application of trained networks to point clouds out of the train or test set is not immediate, which is still an open problem. Instead, our method builds a geometric and probabilistic model to reason registrations case by case, ensuring generality while avoiding the need for annotation.

3. Methodology

Given two point sets $P = \{\mathbf{p}_i \in \mathbb{R}^3 \mid i = 1, 2, \dots, n\}$ and $Q = \{\mathbf{q}_j \in \mathbb{R}^3 \mid j = 1, 2, \dots, m\}$ potentially scanned on the same object under different views, point cloud registration aims to find the optimal rigid transformation $(\mathbf{R}, \mathbf{t}) \in SO(3) \times \mathbb{R}^3$ to align the source point cloud P with the target one Q . We first explore geometric features and then investigate how to integrate them with the hidden Markov model to make the pairwise correspondence more reliable.

3.1. Hidden markov random field

Before introducing the proposed method, let us first provide an overview of the key concepts related to Hidden Markov Random Field (HMRF).

A HMRF is a generalization of a Hidden Markov Model (HMM). It combines concepts from both Hidden Markov Model and Markov random field. Different from HMM which has an underlying Markov chain, HMRF has an underlying Markov random field. Given an observed random variable y , HMRF assumes that the probabilistic nature of y is determined by the unobservable Markov random field z . Given the hidden states z , the random variable y are conditional independent:

$$P(y_i|z, y_{-i}) = P(y_i|z). \quad (1)$$

This conditional independence assumption is crucial for simplifying the modeling and inference processes in HMRFs. It allows for efficient algorithms, such as the Expectation-Maximization (EM) algorithm, to be applied to estimate parameters or infer hidden states. For readers who are interested in conducting more comprehensive studies on HMRF, we recommend referring to [55].

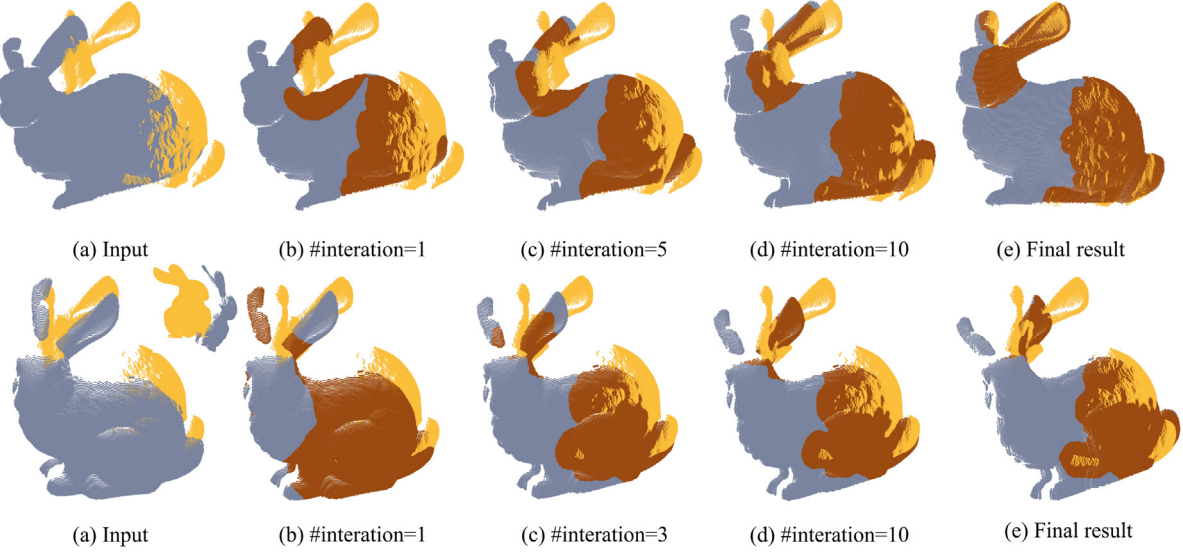


Fig. 3. The iterative process of [23] with the rotation angle $\rho = 15^\circ$ (top) and $\rho = 30^\circ$ (down), where brown region indicates the estimated overlapping part. As observed, [23] converges to a local minimum when the initialization is unsatisfactory ($\rho = 30^\circ$).

3.2. Construction of geometric features

We adopt the *3D structure tensor* or 3D covariance matrix to describe the local geometric features of each point $\mathbf{p}_i \in \mathbb{R}^3$. The mean vector $\mu_i \in \mathbb{R}^3$ of the points in the neighborhood \mathcal{N}_i of \mathbf{p}_i is

$$\mu_i = \frac{1}{|\mathcal{N}_i|} \sum_{\mathbf{p}_k \in \mathcal{N}_i} \mathbf{p}_k, \quad (2)$$

where $\mathcal{N}_i = \{\mathbf{p}_k \in \mathbb{R}^3 | \|\mathbf{p}_k - \mathbf{p}_i\|_2 < r\}$ and $r > 0$ is the support radius. The covariance Σ_i is

$$\Sigma_i = \frac{1}{|\mathcal{N}_i|} \sum_{\mathbf{p}_j \in \mathcal{N}_i} (\mathbf{p}_j - \mu_i)^T (\mathbf{p}_j - \mu_i). \quad (3)$$

Since Σ_i is symmetric and positive definite, we attain $\lambda_1 \geq \lambda_2 \geq \lambda_3 > 0$ after eigenvalue decomposition. We leverage the arithmetic combinations of eigenvalues to describe the local geometric features of each point. The planarity \mathcal{P} , anisotropy \mathcal{A} and curvature \mathcal{C} of \mathbf{p}_i is adopted to accommodate our purpose:

$$\mathcal{P}_{p_i} = \frac{\lambda_2 - \lambda_3}{\lambda_1} \quad \mathcal{A}_{p_i} = \frac{\lambda_1 - \lambda_3}{\lambda_1} \quad \mathcal{C}_{p_i} = \frac{\lambda_3}{\lambda_1 + \lambda_2 + \lambda_3}. \quad (4)$$

3.3. Overlapping region estimation

To distinguish inliers in overlapping regions from outliers, similar to [23], we construct a probabilistic model based on the HMRF. We use \mathbf{z} and \mathbf{y} to represent the hidden field of the unobserved inlier or outlier state and the observed variables, respectively. In the work of [23], they directly choose the distance residual between the closest points as the observed variable \mathbf{y} , which possibly leads to misalignment when the initialization is unsatisfying. Fig. 3 shows the iterative process when applying the distance-based HMRF for registration. As is observed, it performs well under a good initialization with the small rotation angle ($\rho = 15^\circ$); however, as the rotation angle increases ($\rho = 30^\circ$), indicating lower overlapping at initialization, the registration result starts to fail.

Different from the previous approach, in this work, we incorporate geometric features to the observed variable \mathbf{y} and model the hidden Markov random field under higher-dimensional probabilistic distributions. We define the observed variable $\mathbf{y} = [\mathbf{y}_1, \mathbf{y}_2, \mathbf{y}_3, \mathbf{y}_4]^T \in \mathbb{R}^4$, where

$\mathbf{y}_1, \mathbf{y}_2, \mathbf{y}_3, \mathbf{y}_4$ denote the distance, the difference of planarity, anisotropy and curvature between closest points.

Given the observed variables \mathbf{y} , our target is to distinguish the inliers, namely the points in the overlapping region, from the outliers (*i.e.*, the non-overlapping points). The prior hypotheses we made are:

- The inliers typically lie closer to their closest points than the outliers.
- The geometry differences between inliers and their closest points are typically smaller than the outliers.
- The neighbors of the inlier tend to be inliers, while the neighbors of the outlier tend to be outliers.

According to these hypotheses, we adopt two normal distributions of different parameters *i.e.*, *normally distributed for inliers* and *normally distributed for outliers* to model \mathbf{y} . According to [23], the distribution of outliers in different point clouds has its own characteristics and is hard to well fit in all cases by a single distribution. Due to the reason that no distribution outperforms all others in every cases, we choose the most widely used normal distribution because it is simple to estimate within the EM framework. Since unobserved states \mathbf{z} are modeled as a Markov random field, the probability distribution of \mathbf{z} is a Gibbs distribution according to the Hammersley–Clifford theorem [56], *i.e.*,

$$P_G(\mathbf{z}) = W^{-1} \exp(-H(\mathbf{z})), \quad (5)$$

where $W = \sum_{\mathbf{z}} \exp(-H(\mathbf{z}))$ is the normalizing factor and $H(\mathbf{z})$ is the energy function. In our case, we choose the following energy function:

$$H(\mathbf{z}) = -\beta \sum_{i' \sim i} w_{i,i'} z_i z_{i'}, \quad (6)$$

where $w_{i,i'}$ represents the edge weight between z_i and $z_{i'}$ and $\beta \geq 0$ is a parameter relevant to the interactive strength. To simplify computation, we further use the *mean field* to approximate the posterior distribution $P_G(\mathbf{z}|\beta)$. Then the k -dimensional normal distributions are used to present the conditional density f . The detailed approximation steps and the final likelihood of the joint distribution are reported in *Supplemental Material*.

We adopt the *expectation maximization* (EM) algorithm to estimate the maximum likelihood parameters of the model and the hidden state. In E-step, we calculate the hidden state or posterior probability of

the point cloud given the parameters, while in M-step, we calculate the parameters that maximize the expected likelihood. We present the theoretical deduction of the concrete EM steps in *Supplemental Material* to ease the understanding.

After the hidden state estimation, we choose the points \mathbf{p}_i whose hidden state $z_i > 0$ and curvature $C_{p_i} > \tau$ as inliers. Then we optimize the objective function defined in the following section.

3.4. Objective function

The traditional point-to-plane ICP merely takes one normal into the objective function, recently [30] proves the potential of the symmetric function for point cloud registration

$$(\mathbf{p} - \mathbf{q}) \cdot (\mathbf{n}_p + \mathbf{n}_q), \quad (7)$$

where \mathbf{n}_\star is the normal of a point \star . The analysis of the relative position of \mathbf{p} and \mathbf{q} in Eq. (7) gives the following conclusion.

Proposition 1. Points \mathbf{p} and \mathbf{q} and their normals \mathbf{n}_p and \mathbf{n}_q lie in the same cylinder, if and only if Eq. (7) equals to zero.

Theoretical proof is presented in *Supplemental Material*. From the proof, we conclude that without the consideration of the geometric characteristics of each point, all cylinders with arbitrary circle radius satisfy the above condition, and the residual generated by their points get no punishment. However, we mainly want the point pairs with the same geometric characteristic (the local surfaces around both points are the same) to slide between each other without punishment. To this end, we further consider the curvature feature, then the improved objective function is

$$(\mathbf{p} - \mathbf{q}) \cdot (\bar{\mu}_q \mathbf{n}_p + \bar{\mu}_p \mathbf{n}_q), \quad (8)$$

where $\bar{\mu}_p = \mu_p / (\mu_p + \mu_q)$ and $\bar{\mu}_q = \mu_q / (\mu_p + \mu_q)$ are normalized curvatures of \mathbf{p} and \mathbf{q} , respectively. From Eq. (8), we observe that when the curvature $\mu_p = \mu_q$, the objective function is equivalent to the primary symmetric objective function. However, when the curvature $\mu_p \gg \mu_q$, $\bar{\mu}_q \approx 0$, we can approximate the local surface around \mathbf{q} as a plane. In this situation, our proposed objective function (Eq. (8)) is equivalent to the popular point-to-plane function. Therefore, our objective function of the two point clouds \mathcal{P} and \mathcal{Q} is defined as

$$\sum_{i=1}^n \|(\mathbf{R}\mathbf{p}_i - \mathbf{R}^{-1}\mathbf{q}_i + \mathbf{t}) \cdot (\bar{\mu}_{q,i}\mathbf{n}_{p,i} + \bar{\mu}_{p,i}\mathbf{n}_{q,i})\|_2^2. \quad (9)$$

3.5. Stable point-pair sampling

After the determination of the overlapping region between two point clouds, we further propose a point-pair sampling strategy to constrain the uncertainty transformation based on the curvature aware symmetric function, by which the registration becomes more stable in the existence of large percentage of non-feature points. Like [30], we correspond the rotation matrix \mathbf{R} to a fixed axis \mathbf{a} and an angle θ using *Rodrigues rotation formula*, and then adopt linear approximation to transform Eq. (9) as

$$\sum_{i=1}^n \|((\bar{\mathbf{p}}_i - \bar{\mathbf{q}}_i) \cdot \mathbf{n}_i + ((\bar{\mathbf{p}}_i + \bar{\mathbf{q}}_i) \times \mathbf{n}_i) \cdot \tilde{\mathbf{a}} + \mathbf{n}_i \cdot \tilde{\mathbf{t}})\|_2^2, \quad (10)$$

where $\bar{\mathbf{p}}$ and $\bar{\mathbf{q}}$ are the mean value of selected points \mathbf{p}_i and its correspondence \mathbf{q}_i . We have $\bar{\mathbf{p}}_i = \mathbf{p}_i - \bar{\mathbf{p}}$, $\bar{\mathbf{q}}_i = \mathbf{q}_i - \bar{\mathbf{q}}$, $\mathbf{n}_i = \bar{\mu}_{q,i}\mathbf{n}_{p,i} + \bar{\mu}_{p,i}\mathbf{n}_{q,i}$, $\tilde{\mathbf{t}} = \mathbf{t}/\cos\theta$ and $\tilde{\mathbf{a}} = \mathbf{a}\tan\theta$. Considering the last two terms of Eq. (10), we figure out that the i th term of the objective function will change if the given vector $((\bar{\mathbf{p}}_i + \bar{\mathbf{q}}_i) \times \mathbf{n}_i, \mathbf{n}_i)$ is moved by the transformation vector $[\Delta\tilde{\mathbf{a}}^T, \Delta\tilde{\mathbf{t}}^T]$:

$$\Delta e_i = [\Delta\tilde{\mathbf{a}}^T, \Delta\tilde{\mathbf{t}}^T] \begin{bmatrix} (\bar{\mathbf{p}}_i + \bar{\mathbf{q}}_i) \times \mathbf{n}_i \\ \mathbf{n}_i \end{bmatrix}. \quad (11)$$

Algorithm 1: The Proposed Geometrically Stable Point-Pair Sampling

```

Input: Corresponding point pairs  $(\mathbf{p}_i, \mathbf{q}_i)$  together with the
       normal pairs  $(\mathbf{n}_{p,i}, \mathbf{n}_{q,i})$ ,  $i = 1, 2, \dots, n$ ; Desired number of
       point pairs  $m$ ;
Output: Chosen point pairs with their normal  $(\hat{\mathbf{p}}_i, \hat{\mathbf{q}}_i, \mathbf{n}_{\hat{\mathbf{p}}_i}, \mathbf{n}_{\hat{\mathbf{q}}_i})$ ,
        $i = 1, 2, \dots, m$ .
1 Form the covariance matrix  $\mathbf{C}$  and then perform eigenvalue
   decomposition  $\lambda_1 \geq \lambda_2 \geq \dots \geq \lambda_6$ ; The corresponding
   eigenvectors are denoted as  $\mathbf{x}_1, \mathbf{x}_2, \dots, \mathbf{x}_6$ ; Define
    $\mathbf{v}_i = [(\bar{\mathbf{p}}_i + \bar{\mathbf{q}}_i) \times \mathbf{n}_i, \mathbf{n}_i]$ ,  $i = 1, 2, \dots, n$ .
2 for  $k = 1$  to  $6$  do
3   |  $\mathbf{L}_k = [\mathbf{v}_{\sigma_k(1)}, \dots, \mathbf{v}_{\sigma_k(n)}]$  where  $(\mathbf{v}_{\sigma_k(1)} \cdot \mathbf{x}_k)^2 \geq \dots \geq (\mathbf{v}_{\sigma_k(n)} \cdot \mathbf{x}_k)^2$ 
4 end
5 Randomly choose a point pair  $(\hat{\mathbf{p}}_1, \hat{\mathbf{q}}_1)$ ,  $\hat{\mathbf{v}}_1 = [(\hat{\mathbf{p}}_1 + \hat{\mathbf{q}}_1) \times \mathbf{n}_1, \mathbf{n}_1]$  let
    $t_1 = (\hat{\mathbf{v}}_1 \cdot \mathbf{x}_1)^2, t_2 = (\hat{\mathbf{v}}_1 \cdot \mathbf{x}_2)^2, \dots, t_6 = (\hat{\mathbf{v}}_1 \cdot \mathbf{x}_6)^2$ . Delete  $\hat{\mathbf{v}}_1$  from
   the sorted lists  $\mathbf{L}_1, \dots, \mathbf{L}_6$ .
6 for  $j = 2$  to  $m$  do
7   |  $t_s = \min_{i=1, \dots, 6} t_i$ 
8   | Find  $\hat{\mathbf{v}}_j$  from the top of the sorted list  $\mathbf{L}_s$  and choose the
     | corresponding point pair  $(\hat{\mathbf{p}}_j, \hat{\mathbf{q}}_j)$ .
9   |  $t_1 = t_1 + (\hat{\mathbf{v}}_j \cdot \mathbf{x}_1)^2, t_2 = t_2 + (\hat{\mathbf{v}}_j \cdot \mathbf{x}_2)^2, \dots, t_6 = t_6 + (\hat{\mathbf{v}}_j \cdot \mathbf{x}_6)^2$ .
10  | Delete  $\hat{\mathbf{v}}_j$  from  $\mathbf{L}_1, \dots, \mathbf{L}_6$ .
11 end
12 return the chosen point pairs with their normals
    $(\hat{\mathbf{p}}_i, \hat{\mathbf{q}}_i, \mathbf{n}_{\hat{\mathbf{p}}_i}, \mathbf{n}_{\hat{\mathbf{q}}_i})$ ,  $i = 1, 2, \dots, m$ .
```

Eqs. (10) and (11) show that if the vector $[(\bar{\mathbf{p}}_i + \bar{\mathbf{q}}_i) \times \mathbf{n}_i, \mathbf{n}_i]$ is perpendicular to $[\tilde{\mathbf{a}}, \tilde{\mathbf{t}}]$, then the value of the objective function will not change. From the above analysis, we investigate the covariance matrix $\mathbf{C} \in \mathbb{R}^{6 \times 6}$:

$$\mathbf{C} = \begin{bmatrix} (\bar{\mathbf{p}}_1 + \bar{\mathbf{q}}_1) \times \mathbf{n}_1 & \dots & (\bar{\mathbf{p}}_n + \bar{\mathbf{q}}_n) \times \mathbf{n}_n \\ \mathbf{n}_1 & \dots & \mathbf{n}_n \end{bmatrix} \begin{bmatrix} ((\bar{\mathbf{p}}_1 + \bar{\mathbf{q}}_1) \times \mathbf{n}_1)^T & \mathbf{n}_1^T \\ \vdots & \vdots \\ ((\bar{\mathbf{p}}_n + \bar{\mathbf{q}}_n) \times \mathbf{n}_n)^T & \mathbf{n}_n^T \end{bmatrix}. \quad (12)$$

The matrix \mathbf{C} encodes the error variations when the source point cloud \mathcal{P} is moved from its ground-truth location (which is aligned with the target point cloud \mathcal{Q}) by transformation $[\Delta\tilde{\mathbf{a}}, \Delta\tilde{\mathbf{t}}]$:

$$\Delta e = [\Delta\tilde{\mathbf{a}}^T, \Delta\tilde{\mathbf{t}}^T] \mathbf{C} \begin{bmatrix} \Delta\tilde{\mathbf{a}} \\ \Delta\tilde{\mathbf{t}} \end{bmatrix}. \quad (13)$$

Suppose the ordered eigenvalues of \mathbf{C} after eigenvalue decomposition are $\lambda_1 \geq \lambda_2 \geq \dots \geq \lambda_6$ and their corresponding eigenvectors are $\mathbf{x}_1, \mathbf{x}_2, \dots, \mathbf{x}_6$, we find that if the transformation parameters $[\Delta\tilde{\mathbf{a}}, \Delta\tilde{\mathbf{t}}]$ equal to the eigenvector whose corresponding eigenvalue is relatively small, then in this direction the changed error Δe in Eq. (13) will also be small. As is defined in [57], we term this *unconstrained direction*. In order to avoid the possible unconstrained direction, we sample the point pairs to let the condition number $c = \frac{\lambda_1}{\lambda_6}$ of \mathbf{C} as close to one as possible.

Specifically, we define $\mathbf{v}_i = [(\bar{\mathbf{p}}_i + \bar{\mathbf{q}}_i) \times \mathbf{n}_i, \mathbf{n}_i]$, $i = 1, 2, \dots, n$. Then we sort \mathbf{v}_i by its projection value on the eigenvalue \mathbf{x}_k which determines the constraint of \mathbf{v}_i in the direction \mathbf{x}_k , and record it in the list \mathbf{L}_k , $k = 1, 2, \dots, 6$. After modeling the sorted lists $\mathbf{L}_1, \dots, \mathbf{L}_6$, we randomly choose a point pair $(\hat{\mathbf{p}}_1, \hat{\mathbf{q}}_1)$, and let $\hat{\mathbf{v}}_1 = [(\hat{\mathbf{p}}_1 + \hat{\mathbf{q}}_1) \times \mathbf{n}_1, \mathbf{n}_1]$. We then initialize t_1, t_2, \dots, t_6 as $t_1 = (\hat{\mathbf{v}}_1 \cdot \mathbf{x}_1)^2, t_2 = (\hat{\mathbf{v}}_1 \cdot \mathbf{x}_2)^2, \dots, t_6 = (\hat{\mathbf{v}}_1 \cdot \mathbf{x}_6)^2$, and delete $\hat{\mathbf{v}}_1$ from the sorted lists $\mathbf{L}_1, \dots, \mathbf{L}_6$. After initialization, each time we select the point pair from the top of a certain list based on the minimal value of t_1, \dots, t_6 , which can be viewed as the current estimation of the eigenvalues. We then update the value of t_1, \dots, t_6 as $t_1 = t_1 + (\hat{\mathbf{v}}_j \cdot \mathbf{x}_1)^2, t_2 = t_2 + (\hat{\mathbf{v}}_j \cdot \mathbf{x}_2)^2, \dots, t_6 = t_6 + (\hat{\mathbf{v}}_j \cdot \mathbf{x}_6)^2$. The whole procedure is summarized in Algorithm 1.

Table 1

Quantitative results of average RMSE and computation time (in seconds) with different registration methods on Stanford datasets. Bold fonts indicate the best registration accuracy. Our method attains the overall best accuracy along with reasonable runtime.

Methods	Bunny		Armadillo		Dragon		Buddha	
	RMSE	Time	RMSE	Time	RMSE	Time	RMSE	Time
P2P-ICP [11]	0.145	4.53	0.076	0.80	0.057	0.80	0.078	3.35
P2N-ICP [12]	0.132	15.64	0.018	0.53	0.023	1.17	0.054	1.74
GMM [35]	0.286	73.42	0.154	50.39	0.057	56.76	0.217	15.06
CPD [37]	0.238	276.25	0.037	150.80	0.013	158.24	0.027	260.66
HMRF-ICP [23]	0.207	24.30	0.102	8.03	0.037	7.28	0.112	13.88
Ours	0.027	5.42	0.017	6.78	0.018	7.29	0.019	7.86

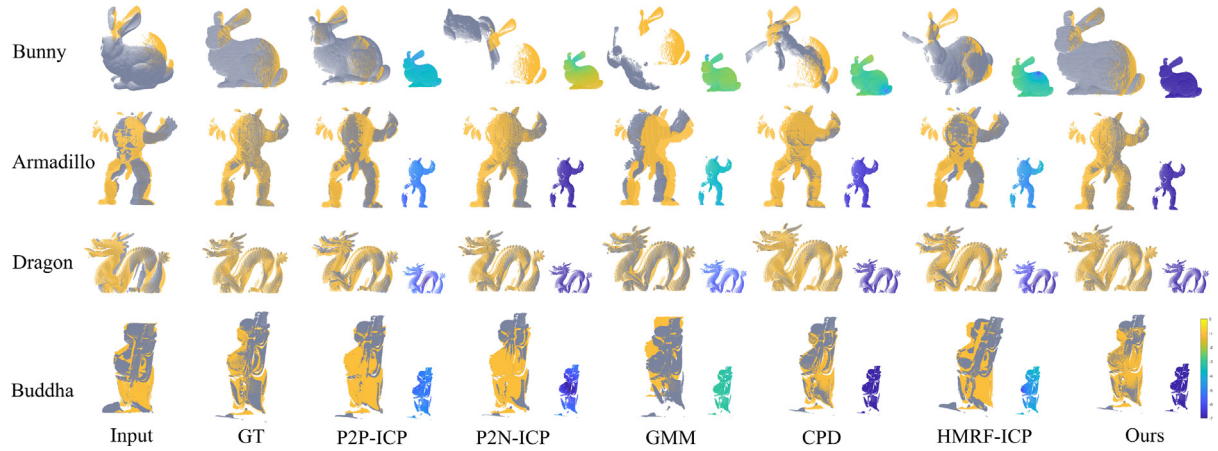


Fig. 4. Registration results on four Stanford scanning datasets. The color-coding in bottom right visualizes the error between the registration results and the ground-truth alignments.

4. Experimental evaluations and discussions

In this section, we perform extensive experiments to evaluate the accuracy, robustness, and efficiency of the proposed method, and compare it with representative state-of-the-art approaches. The implementation of these competitors are publicly available online and their detailed parameter settings are reported in *Supplemental Material*. We adopt the *root mean-squared error* (RMSE) to quantitatively measure the registration quality

$$\text{RMSE} = \sqrt{\frac{1}{N} \sum_{i=1}^N \|\hat{\mathbf{R}}\mathbf{p}_i + \hat{\mathbf{t}} - \mathbf{R}_g\mathbf{p}_i - \mathbf{t}_g\|_2^2}, \quad (14)$$

where $(\hat{\mathbf{R}}, \hat{\mathbf{t}})$ and $(\mathbf{R}_g, \mathbf{t}_g)$ represent the estimated and the ground truth transformations, respectively. We use 10-nearest-neighborhood points for normal calculation. To be statistically representative, we perform 50 experiments for each test and report the average performance of the RMSE and timings. All experiments are executed on a laptop with a 2.50 GHz Intel Core i5-7200 and 4 GB RAM.

4.1. Accuracy test

Firstly, we use four point cloud datasets from the Stanford 3D Scanning Repository [58], *i.e.*, Bunny, Armadillo, Dragon, and Buddha for accuracy test. They are captured by a Cyberware 3030 MS laser scanner with different scanning perspectives, thereby having partial overlappings, as illustrated in the first column of Fig. 4. We compare the proposed method with the Point-to-Point ICP (P2P-ICP) [11], Point-to-Plane ICP (P2N-ICP) [12], HMRF-ICP [23], as well as two popular statistics-based registration methods including GMM [35] and

CPD [37]. The statistical results of each compared method are reported in Table 1. From which, we conclude that the proposed method attains the overall highest accuracy, *i.e.*, the top accuracy on Bunny, Armadillo and Buddha, and the second best accuracy on Dragon. P2P-ICP and P2N-ICP are efficient, but their RMSE are relatively larger than ours. HMRF-ICP consumes more overall time than ours, however, its registration accuracy is still unsatisfying, since its average RMSE are almost 10 times larger than ours. CPD achieves higher accuracy than GMM, especially on Armadillo and Buddha, nevertheless, both of them are subject to highly computational complexity. We present several registration examples in Fig. 4, where the color maps in the lower right indicate the registration deviations under the logarithmic scale.

4.2. Robustness against noise

Subsequently, we assess the robustness of the proposed method against noisy data. To this end, we add a series of Gaussian noise with zero mean and different variance to the source point cloud of the friends dataset [59]. The variance $\sigma^2 \in [0.00, 0.09]$ is varied with the step size equal to $\Delta\sigma^2 = 0.01$. We further compare our method with the robust approaches including Generalized ICP (G-ICP) [15], Fast Global Registration (FGR) [33], Sparse ICP (S-ICP) [32], Fast and Robust ICP (FR-ICP) [19], Symmetric ICP (Sym-ICP) [30], RANSAC [60], as well as deep learning methods including OverlapPredator [61], RegTR [62] and Geometric Transformer (GeoTransformer) [63]. The test results are reported in Fig. 5(a). As observed, the methods P2N-ICP, GMM, G-ICP, RANSAC, Sym-ICP, RegTR and GeoTransformer, showing significant deviations, are more sensitive to noise than the rest ones. With noise level increasing, FGR starts producing large RMSE, indicating that it is less robust to heavy noise. As for OverlapPredator, its performance

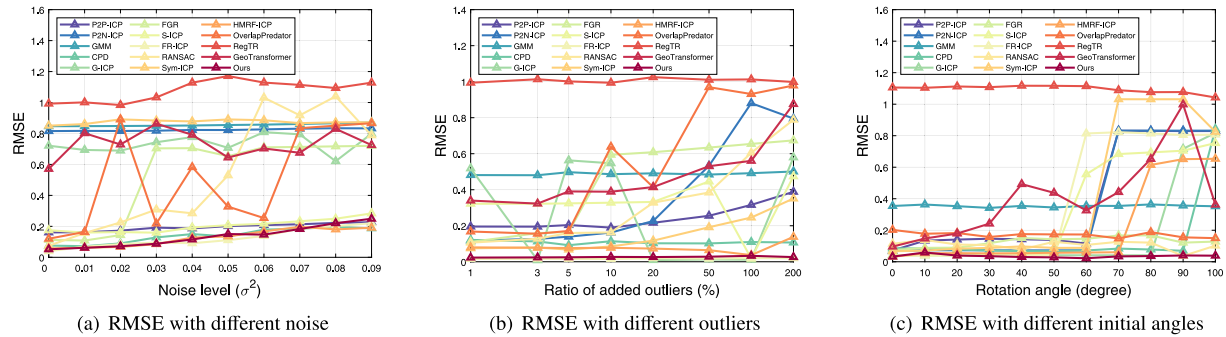


Fig. 5. Statistic of RMSE under different test settings. (a) RMSE with different noise levels, where noise variance σ^2 increases from 0.00 to 0.09. (b) RMSE with different outlier ratios {1%, 3%, 5%, 10%, 20%, 50%, 100%, 200%}. (c) RMSE with different initial angles, where θ ranges from 0° to 100°.

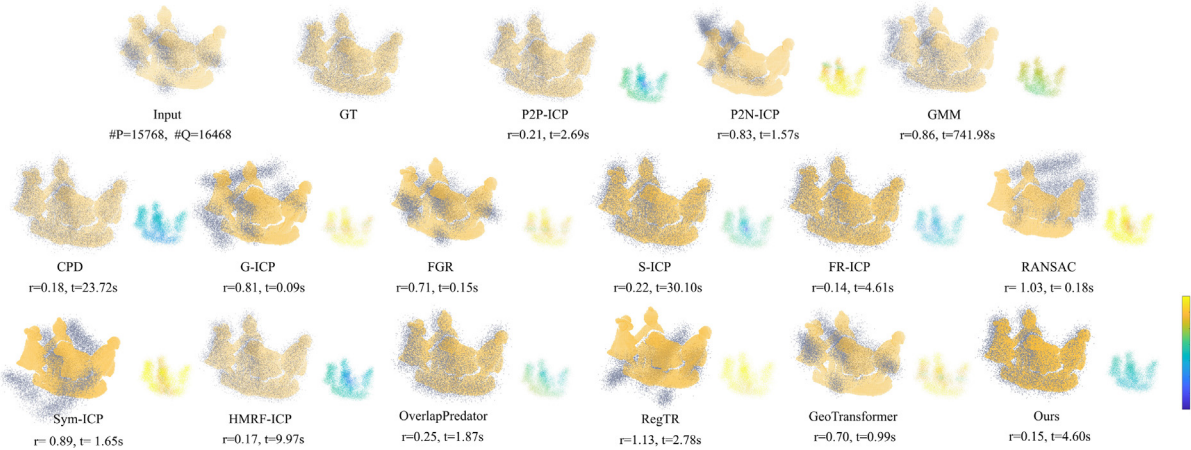


Fig. 6. Comparison samples of different methods under noise contamination $\sigma^2 = 0.06$. The blue and the yellow models represent the source and the target point clouds P, Q , respectively. #P and #Q denote their point size. RMSE (abbreviated as r) and the runtime (t) are reported under each result. The log-scale color map in bottom right visualizes the registration error compared with the ground-truth alignments. Our proposed method attains the second highest registration accuracy with comparable speed.

is unstable while facing different levels of noise, and it tends to get large RMSE under large noise levels. In contrast, CPD, FR-ICP and Ours achieve the overall highest robustness, also, they are substantially stable. Fig. 6 exhibits the comparison samples of all compared methods under the contamination of $\sigma^2 = 0.06$.

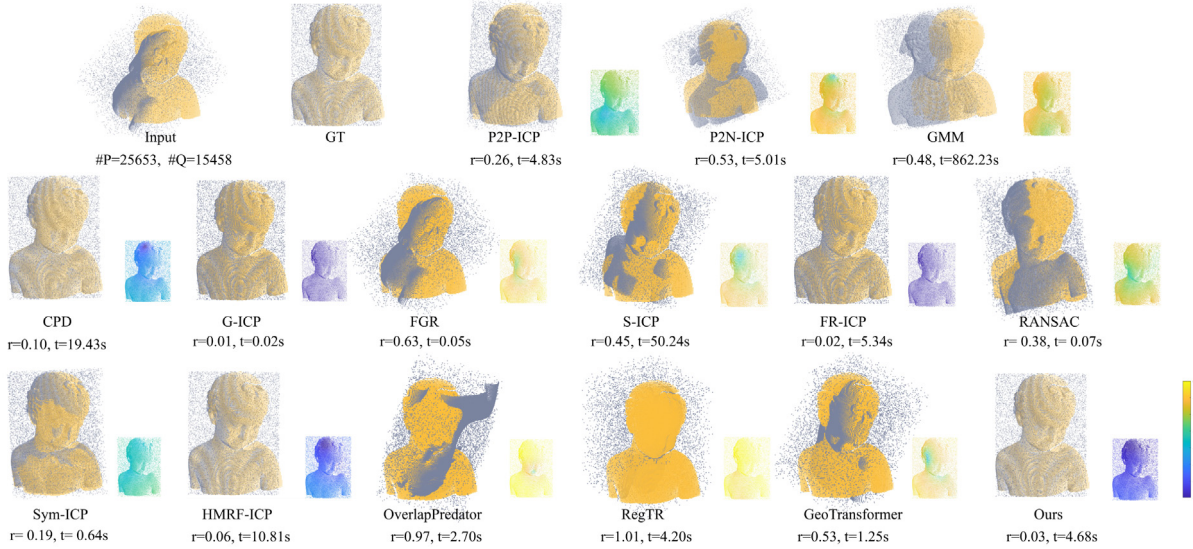
4.3. Robustness against outliers

We also test the influence of outliers for point cloud registration. We adopt the Bimba dataset from the AIM@SHAPE repository [59] for assessment. Some samples are illustrated in Figs. 7(a) and 7(b). Outliers are uniformly distributed within the bounding box of the source point cloud, and the number of them is equal to λN , where N is the amount of the original points, and $\lambda \in \{1\%, 3\%, 5\%, 10\%, 20\%, 50\%, 100\%, 200\%\}$. According to Fig. 5(b), we conclude that FR-ICP and our proposed method are more robust against outliers than competitors. HMRF-ICP has the third-best performance, nevertheless, its time consumption is twice as much as ours. For the other ICP-based methods, they get significant deviations when outliers are over 20%, partially because of the poor initialization and the erroneous correspondence caused by outliers. Outliers have a degree of impact on statistics-based methods since they keep relatively stable performance, which can be attributed to their soft correspondence scheme with probability. However, they show low-quality registration results

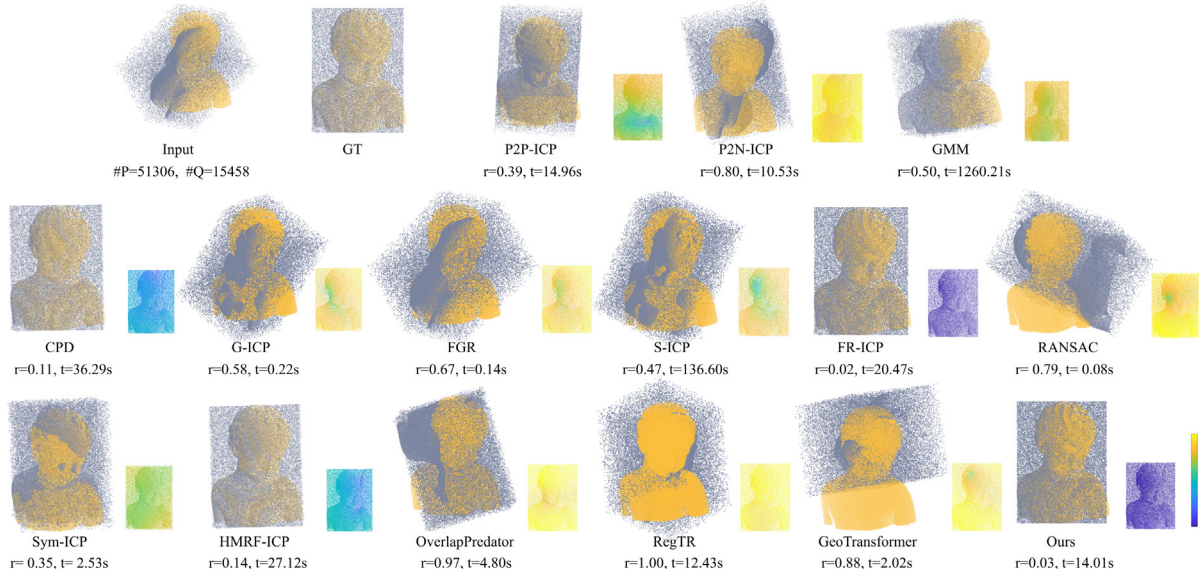
even without the existence of outliers, hence they are preferable to coarse registration tasks. RANSAC is sensitive to outliers especially when two input point clouds are partially overlapped, since it cannot correctly distinguish the overlapped region from high ratio outliers. As for the deep-learning-based methods, their performance is relatively unsatisfactory even under a low ratio of outliers, probably because the models overfit the training data and the insufficient handling of outliers of the network architectures. Instead, our method exhibits highly accurate registration performance. Fig. 7(a) and 7(b) present several comparison samples with $\lambda = 50\%$ and 200% , respectively.

4.4. Initialization impact

Next, we evaluate the performance of all algorithms under different initialization. For this purpose, we exert various rotation angles to the source point cloud of the Berkeley Angel dataset [64], of which the main axis is attained by principle component analysis (PCA). The rotation angle ρ increases from 0° to 100° with the step size equal to 10° . Note that large rotation angles indeed indicate lower overlaps at initialization. We report the test results in Fig. 5(c), where we observe that except GMM and RegTR, all methods perform well when $\rho \leq 30^\circ$. However, as rotation angles become larger, GeoTransformer, FR-ICP and S-ICP return significant errors. P2P-ICP P2N-ICP and Sym-ICP share the similar performance, and their maximum angle tolerance



(a) Registration results under 50% outliers



(b) Registration results under 200% outliers

Fig. 7. Qualitative comparison under the contamination of (a) 50% and (b) 200% outliers. In situation of 50% outliers, G-ICP attains the highest accuracy with the least computation time, while our method also gets promising result. For 200% outliers, our method still successfully registers the point clouds, along with fairly lower RMSE and fast speed.

or breakdown point is 60° . When $\rho > 70^\circ$, HMRF-ICP also generates large deviations, whereas both RANSAC and our method work fairly well even under $\rho = 100^\circ$. Additionally, the proposed method is more stable than CPD, FGR, RANSAC and OverlapPredator, and achieves the highest accuracy, where its RMSE is still less than 0.05 at $\rho = 100^\circ$. We present registration results with the misalignment angle $\rho = 90^\circ$ in Fig. 8.

4.5. Low overlapping test

Previous experiments have demonstrated the promising performance of the proposed method, in this test, we assess its performance with respect to the low overlapping point clouds specially. This case is difficult to handle yet frequently emerges in real-world scenarios. We use two range scans from the TUM RGB-D dataset [65] which

have a low rate of overlapping, as illustrated in Fig. 9. The RMSE and runtime of each method are reported under their registration results in Fig. 9. Results demonstrate that traditional ICP-based methods (P2P-ICP, P2N-ICP and Sym-ICP) suffer from high RMSE in low overlapping situations, hence good initialization is usually required. The statistics-based methods (GMM and CPD) get high RMSE since they also take outliers (points in the non-overlapping region) into consideration. Due to erroneous correspondence or false judgement of outliers, FR-ICP and S-ICP also generate high RMSE. Two of the deep-learning-based methods, namely OverlapPredator and RegTR, targeting at low overlapping registration, get unsatisfactory performance as well probably because of their limited generalization ability. Although G-ICP, FGR, RANSAC, HMRF-ICP and GeoTransformer have relatively lower RMSE compared to the aforementioned methods, their registration results are not accurate enough. However, our proposed method attains the lowest

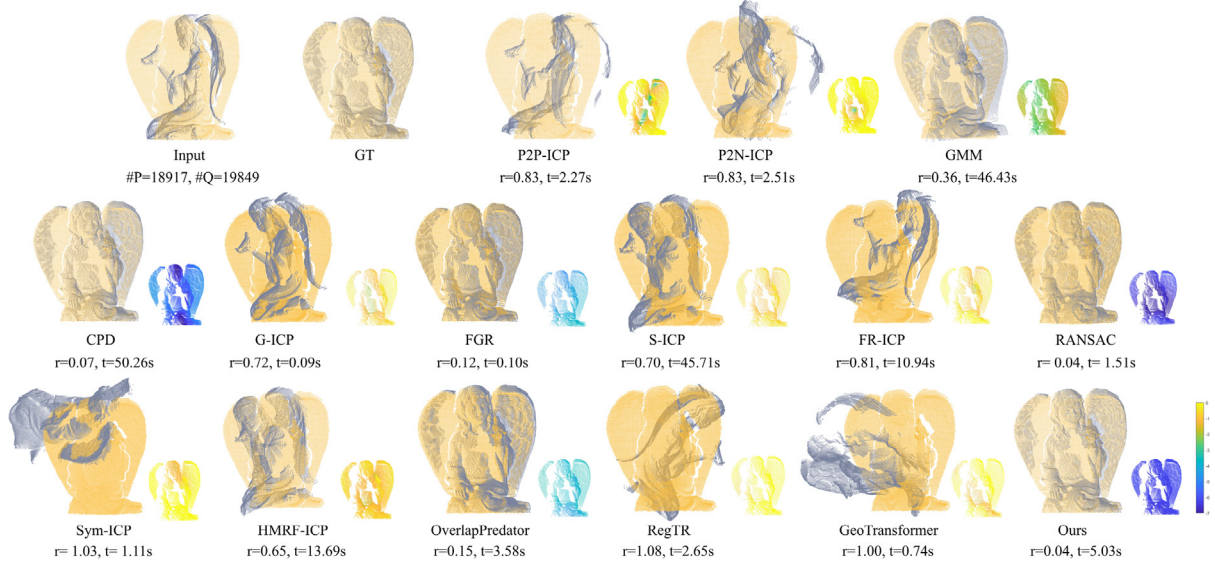


Fig. 8. Comparison samples under the initial rotation angle $\rho = 90^\circ$. Our method outperforms the others with higher registration accuracy, especially under large initial rotation angles or low overlappings.

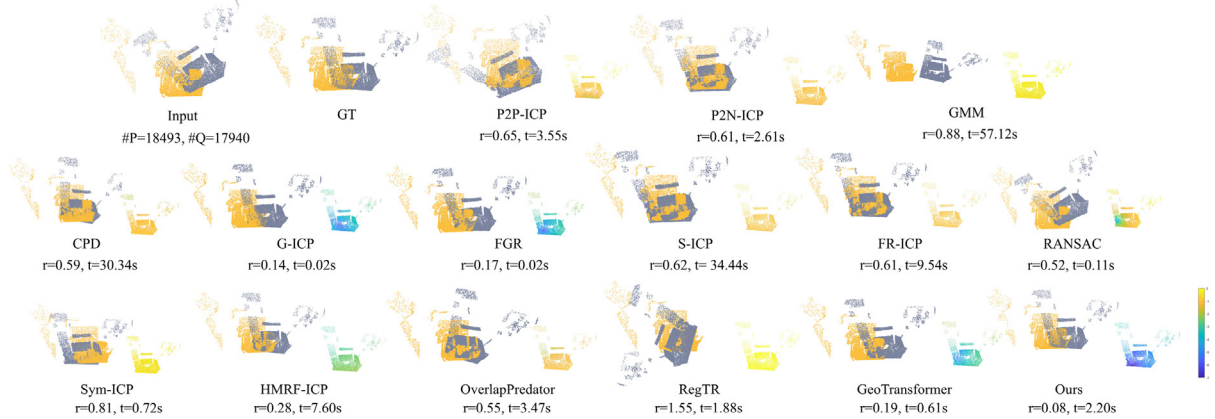


Fig. 9. Registration results of different methods for the low overlapping model. Our method outperforms all competitors with the highest registration accuracy, meanwhile having a reasonable time consumption.

RMSE with comparable convergence speed. The reason is that based on the geometric features, it is able to select the right inliers from input points for registration, meanwhile rejecting outliers in non-overlapping domains. Nevertheless, traditional ICP-based methods treat all points equally as inliers, hence they are prone to resulting in deviations.

Furthermore, we design experiments to analyze the influence of different overlapping rates on registration results. We choose four representative methods in our experiments, namely Sparse ICP, Fast and Robust ICP, HMRF-ICP and Ours, since they are designed to be more robust to low overlapping cases. For comparison, we randomly select eight kinds of point clouds from the TUM RGB-D dataset [65], with their adjacent interval $\alpha \in \{1, 2, 3, 4, 5, 10, 15, 20\}$. For instance, when $\alpha = 5$, the target and source point clouds required registration have indexes $(0, 5), (1, 6), \dots$. The overlapping rate will get much lower as α increases. For each class point cloud, we use 100 frames to ensure the overlapping rate changing from 5% to 100% for test, hence there are in total of 800 point cloud pairs for registration. The overlapping rate of each pair is estimated as follows: The source point \mathbf{p} is considered

to be on the overlapping region A if the distance d_2 to its nearest point of another point cloud $\mathbf{q}_{nearest}$ versus the distance d_1 to the nearest point of its point cloud $\mathbf{p}_{nearest}$ is less than a certain threshold. In our experiments, we set the default tolerance ϵ to be 15 in Eq. (15).

$$\chi_A(\mathbf{p}) = \begin{cases} 1 & \text{if } \frac{d_2}{d_1} < \epsilon \\ 0 & \text{otherwise} \end{cases}, \quad (15)$$

where

$$d_1 := \text{dist}(\mathbf{p}, \mathbf{p}_{nearest}) \quad d_2 := \text{dist}(\mathbf{p}, \mathbf{q}_{nearest}) \quad (16)$$

The three rows in Fig. 10 show the influence of different overlapping rates on RMSE, translation error, and rotation error, respectively. We figure out that when the overlapping rate is high, all methods work well and FR-ICP has the minimum average RMSE. However, when the overlapping rate decreases, its performance deteriorates rapidly. Its median RMSE exceeds 0.5 when the overlapping rate is less than 70%. HMRF-ICP and our method perform well at moderate overlapping

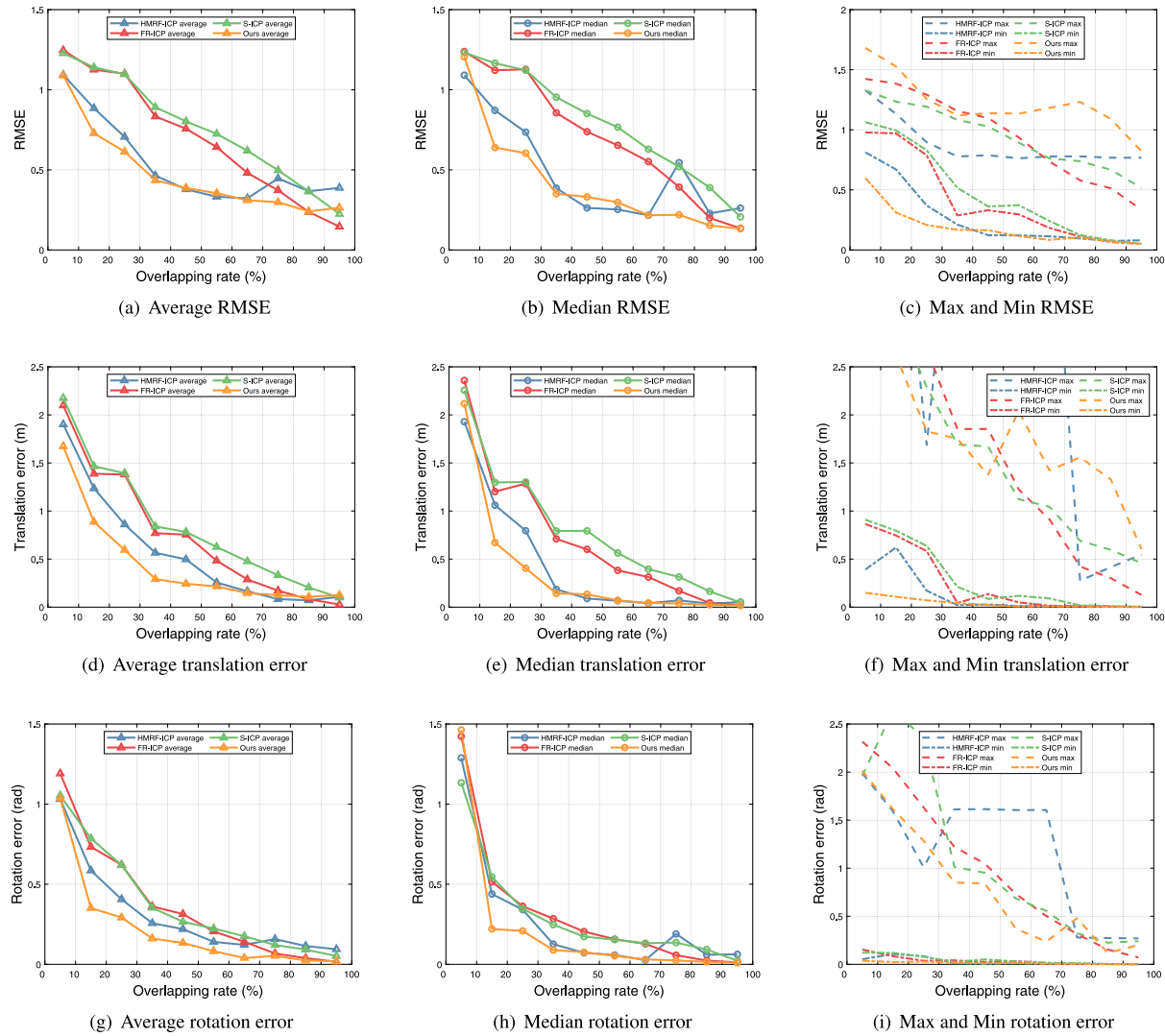


Fig. 10. Quantitative results of RMSE, translation error, and rotation error under a set of overlapping rates. We present the average, median, and maximum-minimum registration deviations on the first, second, and third column, respectively. As observed, the error increases when the overlapping rate decreases.

rate, but our method has lower translation error and rotation error in average. When overlapping rate is below 20%, no methods perform fairly well on all cases, but our method can still work well on some cases since the minimum RMSE, translation error, and rotation error of our method are the lowest compared with the others. Therefore, we conclude that our method has wider convergence basin than competitors under low overlapping settings. We present several samples with different overlapping rates in Fig. 11.

4.6. Sequence point cloud test

In this section, we evaluate the performance of each method on sequence point clouds. We adopt the ETH laser dataset [66] and the KITTI dataset [67] for test. For the ETH laser dataset, the *Apartment* sequence that contains 45 point clouds are used. We align the adjacent point cloud pairs in the sequence and calculate the RMSE as well as the running time. Since the number of points is too large in raw data, we randomly sample 20% candidate points for registration. However, methods like CPD and GMM still suffer from fairly high computational complexity, hence the number of candidate points for these two methods is further reduced to seven thousand. From the

result presented in Fig. 12, we observe that our method and FR-ICP enable high registration accuracy, meanwhile ours is faster than FR-ICP and the others lead to relatively large deviations. For the KITTI dataset, we align the point clouds in the sequence whose index intervals are 1, 4 and 8. The larger index interval indicates the lower overlapping rate. The registration results are presented in Fig. 14. From which, we conclude that when the two point clouds have high overlapping, almost all approaches work well as illustrated in Fig. 14(a), where red boxes indicate relatively large deviations. Nevertheless, with the interval increase, *i.e.*, the decrease of overlapping between two point clouds, more methods start generating registration error, as shown in Fig. 14(b). However, our proposed algorithm still attains accurate results, even under the interval equal to 8, as presented in Fig. 14(c), of which the circles indicate the zoom-in registration.

4.7. One-iteration convergence test

To assess the efficacy of the proposed objective function, we conduct the following experiment. Given two partially overlap point clouds, we transform the source point cloud from its ground-truth position and apply a single iteration of ICP to the source point cloud based on

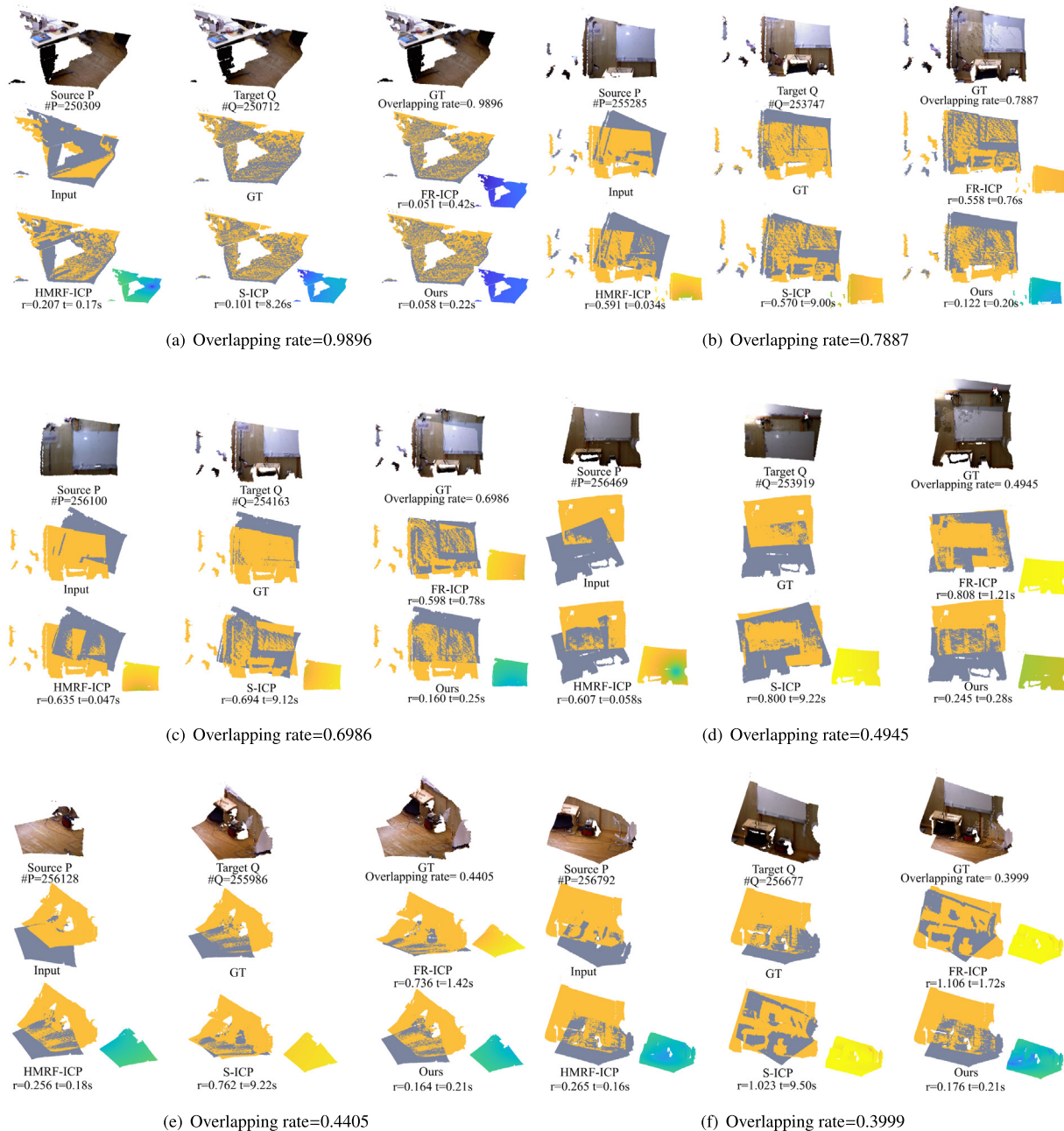


Fig. 11. Registration results with different overlapping rates. The first row illustrates the original point clouds attained based on RGB images and depth maps. The second row and the third row show the registration results of different methods and their log-scale color coding. As observed, our proposed method achieves the most reliable registration under various low overlapping rates.

different objective functions. We record the RMSE of two point clouds both before and after one iteration to evaluate its convergence speed.

We compare three ICP-based objective functions, namely symmetric ICP [30], RSICP [68] and the proposed objective function. The result of aligning bun000 to bun090, two point clouds from Stanford bunny model, is shown in Fig. 13. From the result, we can conclude that when two point clouds have relatively small misalignment, RSICP has the fastest convergence. However, when the misalignment becomes larger, its error reduction capacity in one iteration decreases, and the symmetric metric and the proposed metric have better performance. Moreover, the proposed metric has a higher convergence speed than the symmetric metric before the error reaches 0.15. The symmetric metric

has the best performance for the large dis-alignment and the proposed metric achieves a comparable convergence rate.

5. Conclusions and future research

We presented a novel and robust method for accurate registration of challenging low overlapping point clouds. We integrate geometric features with the probabilistic model hidden Markov random field to effectively infer overlapping regions between two point clouds and depress outlier contamination. We prove a necessary and sufficient condition when the preliminary symmetric function equals to zero, analyze its shortcomings, and introduce a curvature-aware symmetric function

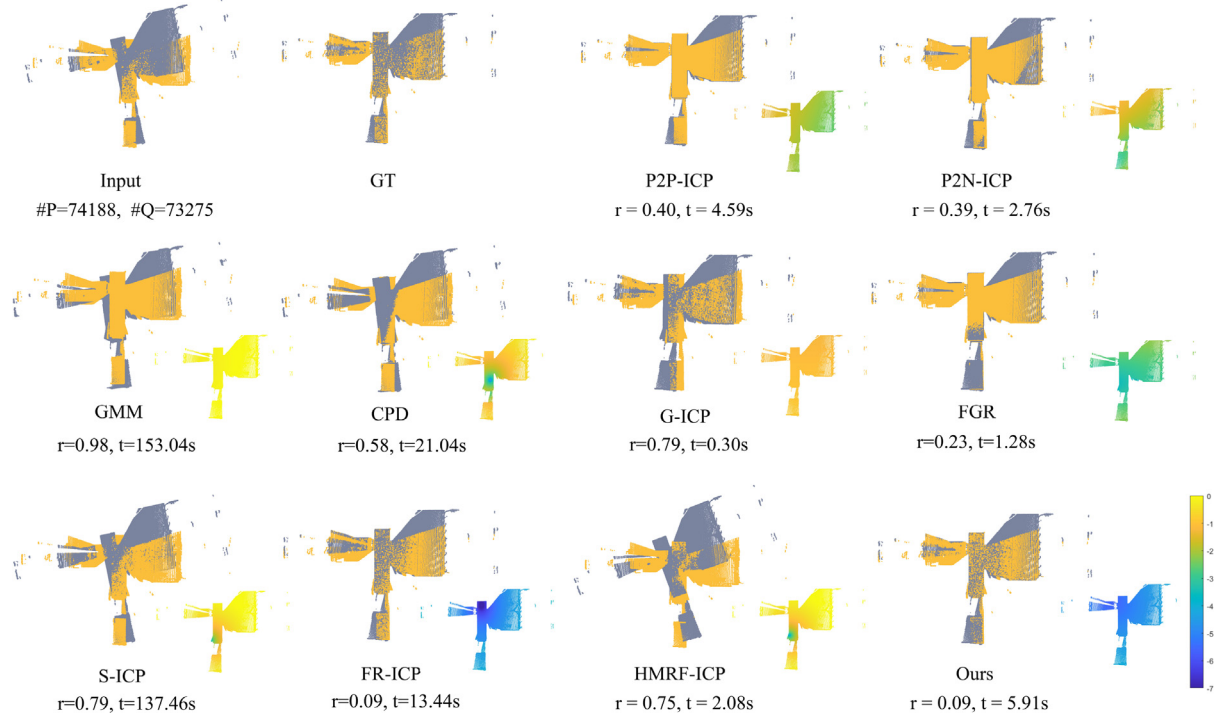


Fig. 12. Registration results of different methods on the ETH dataset. Our method and FR-ICP achieve the best performance, whereas our method consumes twofold less runtime as FR-ICP.

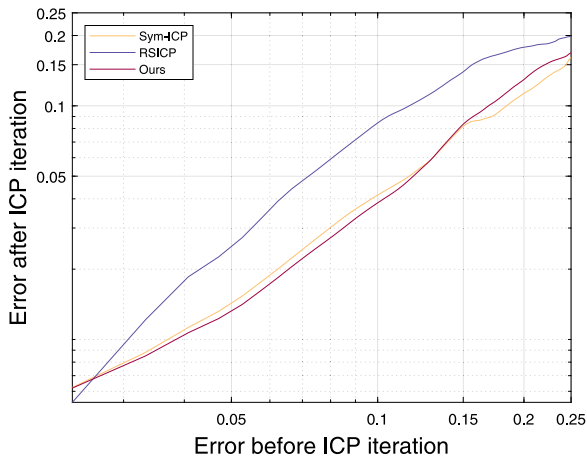


Fig. 13. One-iteration convergence test on the objective functions of symmetric icp, RSICP and the proposed objective function. The ground-truth RMSE values before and after the ICP iteration are graphically represented on a log-log plot, with the x-axis and y-axis denoting the respective pre- and post-iteration RMSE values. The proposed objective function results in faster decrease of RMSE at each iteration.

to make the point correspondence more discriminative, thereby resulting in more accurate registration. Additionally, we introduce a linear approximation to the proposed objective function and then involve it into a geometrically stable sampling framework to achieve more stable transformations.

We assess the proposed method and compare it with representative state-of-the-art approaches on noisy, outlier-contaminated, various initialization, and low overlapping settings, where results demonstrate that the proposed method outperforms competitors with higher

accuracy and robustness along with reasonable time consumption, especially on low overlapping scenarios.

The currently proposed registration framework is limited to pairwise low overlapping point clouds, in the future, we plan to generalize it to multi-view low overlapping cases. For such quite challenging assignments, to avoid error accumulation between multiple transformations, we can theoretically formalize the task as a clustering problem and then explore solutions by probabilistic graph models.

CRediT authorship contribution statement

Jieyin Yang: Software. **Mingyang Zhao:** Writing – original draft. **Yingrui Wu:** Software. **Xiaohong Jia:** Funding acquisition, Supervision.

Declaration of competing interest

The authors declare that they have no known competing financial interests or personal relationships that could have appeared to influence the work reported in this paper.

Data availability

Data will be made available on request.

Acknowledgements

This work is supported by National Key R&D Program of China (2021YFB1715900), the National Natural Science Foundation of China (12022117), and the CAS Project for Young Scientists in Basic Research (YSBR-034).

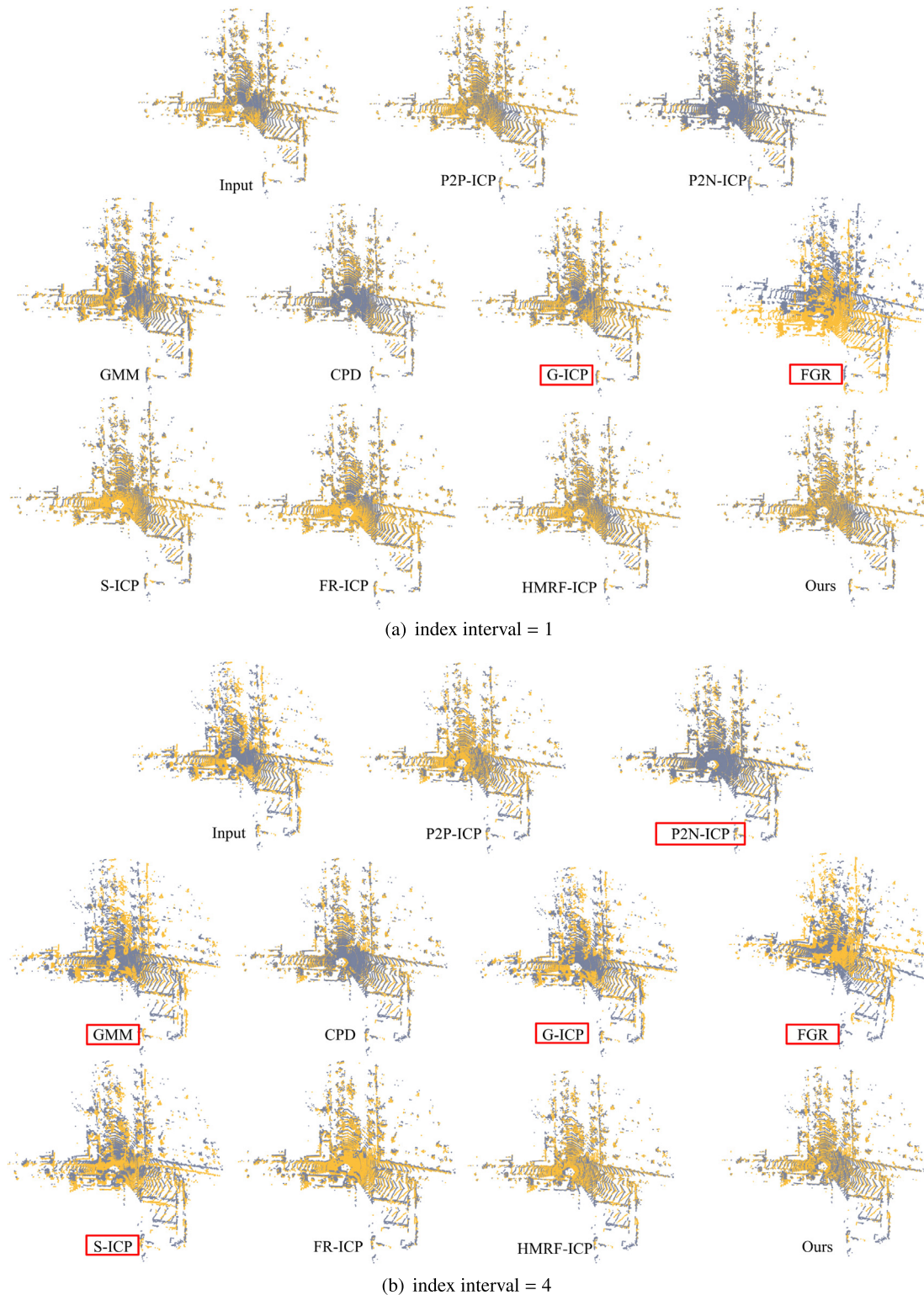
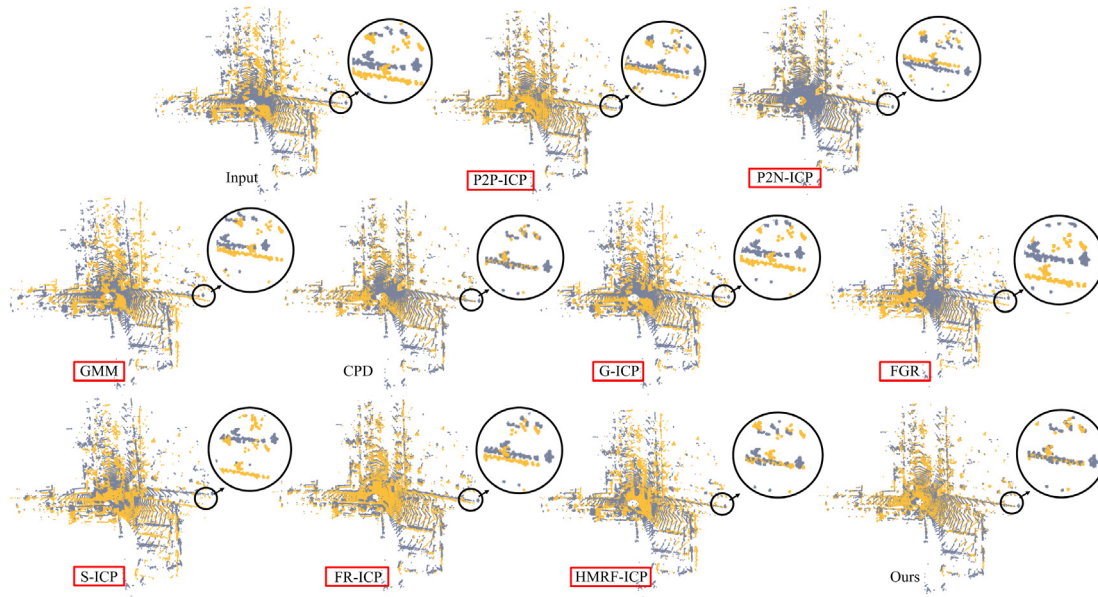


Fig. 14. Registration results of the KITTI dataset with the index interval equal to 1, 4 and 8. Red boxes indicate methods that have relatively large deviations and circles are the zoom-in results.



(c) index interval = 8

Fig. 14. (continued).

Appendix A. Supplementary data

Supplementary material related to this article can be found online at <https://doi.org/10.1016/j.cag.2023.12.003>.

References

- [1] Xie Qian, Zhang Yiming, Cao Xuanming, Xu Yabin, Lu Dening, Chen HongHua, et al. Part-in-whole point cloud registration for aircraft partial scan automated localization. *Comput Aided Des* 2021;137:103042.
- [2] Cao Xuanming, Gong Xiaoxi, Xie Qian, Huang Jiayi, Xu Yabin, Liu Yuanpeng, et al. Raw scanned point cloud registration with repetition for aircraft fuel tank inspection. *Comput Aided Des* 2022;144:103164.
- [3] Sun Wei, Starly Binil, Nam Jae, Darling Andrew. Bio-CAD modeling and its applications in computer-aided tissue engineering. *Comput Aided Des* 2005;37(11):1097–114.
- [4] Liu Yang, Pottmann Helmut, Wang Wenping. Constrained 3D shape reconstruction using a combination of surface fitting and registration. *Comput Aided Des* 2006;38(6):572–83.
- [5] Huang Yunbao, Qian Xiaoping, Chen Shiliang. Multi-sensor calibration through iterative registration and fusion. *Comput Aided Des* 2009;41(4):240–55.
- [6] Yang Heng, Carbone Luca. In perfect shape: Certifiably optimal 3D shape reconstruction from 2D landmarks. In: Proc. IEEE conf. comput. vis. pattern recog. 2020, p. 621–30.
- [7] Ip Cheuk Yiu, Gupta Satyandra K. Retrieving matching CAD models by using partial 3D point clouds. *Comput Aided Des Appl* 2007;4(5):629–38.
- [8] Thomson C, Apostolopoulos G, Backes D, Boehm J. Mobile laser scanning for indoor modelling. *ISPRS J PhotoGramm* 2013;5(W2):66.
- [9] Fiorucci Marco, Khoroshiltseva Marina, Pontil Massimiliano, Travaglia Arianna, Del Bue Alessio, James Stuart. Machine learning for cultural heritage: A survey. *Pattern Recognit Lett* 2020;133:102–8.
- [10] Li Jiayuan. A practical O (N²) outlier removal method for point cloud registration. *IEEE Trans Pattern Anal Mach Intell* 2021.
- [11] Besl Paul J, McKay Neil D. Method for registration of 3-D shapes. In: Sensor fusion IV: control paradigms and data structures, Vol. 1611. International Society for Optics and Photonics; 1992, p. 586–606.
- [12] Chen Yang, Medioni Gérard. Object modelling by registration of multiple range images. *Image Vis Comput* 1992;10(3):145–55.
- [13] Umeyama Shinji. Least-squares estimation of transformation parameters between two point patterns. *IEEE Trans Pattern Anal Mach Intell* 1991;13(04):376–80.
- [14] Walker Michael W, Shao Lejun, Volz Richard A. Estimating 3-D location parameters using dual number quaternions. *Comput Gr Image Process* 1991;54(3):358–67.
- [15] Segal Aleksandr, Haehnel Dirk, Thrun Sebastian. Generalized-ICP. In: Robot. sci. syst. Vol. 2. No. 4. Seattle, WA; 2009, p. 435.
- [16] Serafin Jacopo, Grisetti Giorgio. NICP: Dense normal based point cloud registration. In: IEEE/RSJ int. conf. intell. robot. syst. IEEE; 2015, p. 742–9.
- [17] Granger Sébastien, Pennec Xavier. Multi-scale EM-ICP: A fast and robust approach for surface registration. In: Proc. Eur. conf. comput. vis. Springer; 2002, p. 418–32.
- [18] Wu Zongze, Chen Hongchen, Du Shaoyi, Fu Minyue, Zhou Nan, Zheng Nanning. Correntropy based scale ICP algorithm for robust point set registration. *Pattern Recognit* 2019;93:14–24.
- [19] Zhang Juyong, Yao Yuxin, Deng Bailin. Fast and robust iterative closest point. *IEEE Trans Pattern Anal Mach Intell* 2021.
- [20] Wang Gang, Chen Yufei. Robust feature matching using guided local outlier factor. *Pattern Recognit* 2021;117:107986.
- [21] Wu Yue, Liu Yibo, Gong Maoguo, Gong Peiran, Li Hao, Tang Zedong, et al. Multi-view point cloud registration based on evolutionary multitasking with bi-channel knowledge sharing mechanism. *IEEE Trans Emerg Top Comput Intell* 2022;7(2):357–74.
- [22] Zhou Lei, Zhu Siyu, Luo Zixin, Shen Tianwei, Zhang Runze, Zhen Mingmin, et al. Learning and matching multi-view descriptors for registration of point clouds. In: Proc. Eur. conf. comput. vis. 2018, p. 505–22.
- [23] Stechschulte John, Ahmed Nisar, Heckman Christoffer. Robust low-overlap 3-D point cloud registration for outlier rejection. In: IEEE int. conf. robot. autom. 2019, p. 7143–9.
- [24] Wu Yue, Zhang Yue, Ma Wenping, Gong Maoguo, Fan Xiaolong, Zhang Mingyang, et al. RORNet: Partial-to-partial registration network with reliable overlapping representations. *IEEE Trans Neural Netw Learn Syst* 2023.
- [25] Chatzis Sotirios P, Varvarigou Theodora A. A fuzzy clustering approach toward hidden Markov random field models for enhanced spatially constrained image segmentation. *IEEE Trans Fuzzy Syst* 2008;16(5):1351–61.
- [26] Tam Gary KL, Cheng Zhi-Quan, Lai Yu-Kun, Langbein Frank C, Liu Yonghuai, Marshall David, et al. Registration of 3D point clouds and meshes: A survey from rigid to nonrigid. *IEEE Trans Vis Comput Graphics* 2012;19(7):1199–217.
- [27] Bouaziz Sofien, Tagliasacchi Andrea, Li Hao, Pauly Mark. Modern techniques and applications for real-time non-rigid registration. In: ACM trans. graph. 2016, p. 1–25.
- [28] Wang Wenping, Pottmann Helmut, Liu Yang. Fitting B-spline curves to point clouds by curvature-based squared distance minimization. *ACM Trans Graph* 2006;25(2):214–38.
- [29] Pottmann Helmut, Huang Qi-Xing, Yang Yong-Liang, Hu Shi-Min. Geometry and convergence analysis of algorithms for registration of 3D shapes. *Int J Comput Vis* 2006;67(3):277–96.
- [30] Rusinkiewicz Szymon. A symmetric objective function for ICP. *ACM Trans Graph* 2019;38(4):1–7.
- [31] Hontani Hidekata, Matsuno Takamiti, Sawada Yoshihide. Robust nonrigid ICP using outlier-sparsity regularization. In: Proc. IEEE conf. comput. vis. pattern recog. 2012, p. 174–81.
- [32] Bouaziz Sofien, Tagliasacchi Andrea, Pauly Mark. Sparse iterative closest point. In: Comput. graph. forum. Vol. 32. No. 5. Wiley Online Library; 2013, p. 113–23.
- [33] Zhou Qian-Yi, Park Jaesik, Koltun Vladlen. Fast global registration. In: Proc. Eur. conf. comput. vis. 2016, p. 766–82.
- [34] Fusello Andrea, Castellani Umberto, Ronchetti Luca, Murino Vittorio. Model acquisition by registration of multiple acoustic range views. In: Proc. Eur. conf. comput. vis. 2002, p. 805–19.

- [35] Jian Bing, Vemuri Baba C. Robust point set registration using gaussian mixture models. *IEEE Trans Pattern Anal Mach Intell* 2010;33(8):1633–45.
- [36] Tabib Wennie, O’Meadhra Cormac, Michael Nathan. On-manifold gmm registration. *Proc IEEE Robot Autom Lett* 2018;3(4):3805–12.
- [37] Myronenko Andriy, Song Xubo. Point set registration: Coherent point drift. *IEEE Trans Pattern Anal Mach Intell* 2010;32(12):2262–75.
- [38] Danelljan Martin, Meneghetti Giulia, Khan Fahad Shahbaz, Felsberg Michael. A probabilistic framework for color-based point set registration. In: Proc. IEEE conf. comput. vis. pattern recog. 2016, p. 1818–26.
- [39] Lawin Felix Järemo, Danelljan Martin, Khan Fahad Shahbaz, Forssén Per-Erik, Felsberg Michael. Density adaptive point set registration. In: Proc. IEEE conf. comput. vis. pattern recog. 2018, p. 3829–37.
- [40] Hirose Osamu. A Bayesian formulation of coherent point drift. *IEEE Trans Pattern Anal Mach Intell* 2020.
- [41] Zhao Mingyang, Huang Xiaoshui, Jiang Jingren, Mou Luntian, Yan Dong-Ming, Ma Lei. Accurate registration of cross-modality geometry via consistent clustering. *IEEE Trans Vis Comput Graphics* 2023.
- [42] Fischler Martin A, Bolles Robert C. Random sample consensus: a paradigm for model fitting with applications to image analysis and automated cartography. *Commun ACM* 1981;24(6):381–95.
- [43] Torr Philip Hilaire, Nasuto Slawomir J, Bishop John Mark. Napsac: High noise, high dimensional robust estimation-it’s in the bag. In: Proc. Brit. mach. vis. conf. Vol. 2. 2002, p. 3.
- [44] Barath Daniel, Ivashechkin Maksym, Matas Jiri. Progressive NAPSAC: sampling from gradually growing neighborhoods. 2019, arXiv preprint [arXiv:1906.02295](https://arxiv.org/abs/1906.02295).
- [45] Li Jiayuan, Hu Qingwu, Ai Mingyao. Point cloud registration based on one-point ransac and scale-annealing biweight estimation. *IEEE Trans Geosci Remote Sens* 2021;59(11):9716–29.
- [46] Li Jiayuan, Hu Qingwu, Ai Mingyao. GESAC: Robust graph enhanced sample consensus for point cloud registration. *ISPRS Ann Photogram Remote Sens Spatial Inf Sci* 2020;167:363–74.
- [47] Li Jiayuan, Shi Pengcheng, Hu Qingwu, Zhang Yongjun. QGORE: Quadratic-time guaranteed outlier removal for point cloud registration. *IEEE Trans Pattern Anal Mach Intell* 2023.
- [48] Aoki Yasuhiro, Goforth Hunter, Srivatsan Rangaprasad Arun, Lucey Simon. Pointnetlk: Robust & efficient point cloud registration using pointnet. In: Proc. IEEE conf. comput. vis. pattern recog. 2019, p. 7163–72.
- [49] Qi Charles R, Su Hao, Mo Kaichun, Guibas Leonidas J. Pointnet: Deep learning on point sets for 3d classification and segmentation. In: Proc. IEEE conf. comput. vis. pattern recog. 2017, p. 652–60.
- [50] Lucas Bruce D, Kanade Takeo. An iterative image registration technique with an application to stereo vision. In: Int. joint conf. artificial intell. Vol. 2. 1981, p. 674–9.
- [51] Wang Yue, Solomon Justin M. Deep closest point: Learning representations for point cloud registration. In: Proc. IEEE int. conf. comput. vis. 2019, p. 3523–32.
- [52] Lu Weixin, Wan Guowei, Zhou Yao, Fu Xiangyu, Yuan Pengfei, Song Shiyu. DeepVCP: An end-to-end deep neural network for point cloud registration. In: Proc. IEEE int. conf. comput. vis. 2019, p. 12–21.
- [53] Choy Christopher, Dong Wei, Koltun Vladlen. Deep global registration. In: Proc. IEEE conf. comput. vis. pattern recog. 2020, p. 2514–23.
- [54] Ao Sheng, Hu Qingyong, Wang Hanyun, Xu Kai, Guo Yulan. BUFFER: Balancing accuracy, efficiency, and generalizability in point cloud registration. In: Proc. IEEE conf. comput. vis. pattern recog. 2023, p. 1255–64.
- [55] Chatzis Sotirios P, Tschepenakis Gabriel. The infinite hidden Markov random field model. *IEEE Trans Neural Netw* 2010;21(6):1004–14.
- [56] Clifford Peter. Markov random fields in statistics. *Disorder Phys Syst* 1990;19–32.
- [57] Gelfand Natasha, Ikemoto Leslie, Rusinkiewicz Szymon, Levoy Marc. Geometrically stable sampling for the ICP algorithm. In: Int. conf. on 3d dig. imaging and modeling. IEEE; 2003, p. 260–7.
- [58] The Stanford 3D Scanning Repository. [Online]. Available. <http://graphics.stanford.edu/data/3Dscanrep/>.
- [59] The KITTI Vision Benchmark Suite. [Online]. Available. <http://www.cvlibs.net/datasets/kitti/>.
- [60] Bolles Robert C, Fischler Martin A. A RANSAC-based approach to model fitting and its application to finding cylinders in range data. In: Int. joint conf. artificial intell. 1981, p. 637–43, 1981.
- [61] Huang Shengyu, Gojcic Zan, Usvyatsov Mikhail, Wieser Andreas, Schindler Konrad. Predator: Registration of 3d point clouds with low overlap. In: Proc. IEEE conf. comput. vis. pattern recog. 2021, p. 4267–76.
- [62] Yew Zi Jian, Lee Gim Hee. Regtr: End-to-end point cloud correspondences with transformers. In: Proc. IEEE conf. comput. vis. pattern recog. 2022, p. 6677–86.
- [63] Qin Zheng, Yu Hao, Wang Changjian, Guo Yulan, Peng Yuxing, Xu Kai. Geometric transformer for fast and robust point cloud registration. In: Proc. IEEE conf. comput. vis. pattern recog. 2022, p. 11143–52.
- [64] Kolluri Ravikrishna, Shewchuk Jonathan Richard, O’Brien James F. Spectral surface reconstruction from noisy point clouds. In: ACM symp. geom. process. 2004, p. 11–21.
- [65] Sturm Jürgen, Engelhard Nikolas, Endres Felix, Burgard Wolfram, Cremer Daniel. A benchmark for the evaluation of RGB-D SLAM systems. In: IEEE/RSJ int. conf. intell. robot. syst. 2012, p. 573–80.
- [66] Terrestrial Laser Scanner Point Clouds. [Online]. Available. https://prs.igp.ethz.ch/research/completed_projects.html.
- [67] AIM@SHAPE Shape Repository. [Online]. Available. <http://visionair.ge.imati.cnr.it/ontologies/shapes/>.
- [68] Li Jiayuan, Hu Qingwu, Zhang Yongjun, Ai Mingyao. Robust symmetric iterative closest point. *ISPRS Ann Photogram Remote Sens Spatial Inf Sci* 2022;185:219–31.